The Role of the Zagros Suture on Three Dimensional Deformation Pattern in Eghlid-Deh Bid Area of Iran

K. Sarkarinejad and A. Barjasteh[*]

Department of Earth Sciences, College of Sciences, Shiraz University, Shiraz, Islamic Republic of Iran

Abstract

Deformation pattern of the northeastern part of the Iranian-Arabian collision zone (i.e., mainly Sanandaj-Sirjan Belt or Zone) is the main concern of this paper. Here, we investigate the stress distribution and displacement pattern of Eghlid-Deh Bid area as affected by the position of Zagros suture using a three dimensional mechanical model. The modeled area is located between the Zagros Thrust Fault on the west and Deh Shir-Baft Fault in the east as its edges. The model is composed of 3 layers: the upper two layers represent the upper brittle and lower ductile crusts of the collided continent and the lowest layer represents lithospheric mantle. The bounding major faults are treated as vertical sides of the model. We introduced a discontinuity parallel with the Zagros Thrust Line at two different locations at the western margin and in the middle of the model to simulate Zagros suture to investigate its debated position and role on the deformation history in the area. Our results showed that stress and displacement patterns are fairly affected and disturbed by its position in the two cases. It could also have partitioned deformation across the study area particularly due to its marginal position. The modeled pattern of stress and displacement fields are both totally comparable with plate boundary shear zones demonstrating dextral transpression and more consistent with a suture zone located at or very close to the Zagros Thrust Line place. Such a conclusion is in agreement with recent field surveys including micro and macro-tectonic data.

Keywords: Zagros suture zone; Sanandaj-Sirjan zone; Numerical modeling; Eghlid-Deh Bid region

Introduction

Shear zones with plate scale size are important features in geology as they define boundaries of the plates [40, Fig. 7]. They behave as ductile zones and getting insight into their mechanism of formation and evolution could help understanding plate tectonics [20]. In spite of relative availability and variability of methods to study brittle fault zones, ductile shear zones are much more difficult to study regarding to their limited evidence in their exposures on the Earth. Their shearing can be observed indirectly only in special

* Corresponding author, Tel.: +98(611)3369185, Fax: +98(611)3737164, E-mail: barjasteh@hotmail.com

circumstance where anomalous heat transfer [34] or earthquake rupturing occurred [81,47,92,68,91]. In this way, modeling approach will be powerful and versatile [14,86,23,35] for the purposes of studies. Such an approach may include laboratory analogue modeling [e.g., 26,71] or mechanical numerical analysis [e.g., 17]. Due to the obliquity of convergent vector between the Arabian and Iranian Plates, such shear zones can occur within the interior of the Iranian Plate at least as local shear zones. In this regard, our study area (Eghlid–Deh Bid) located within Sanandaj-Sirjan Metamorphic Belt (SSB) (Stocklin 1968a) can be considered as a shear zone [e.g., 81,13,58] taking into account its boundaries that are specified by Zagros Thrust Fault and Deh Shir-Baft Fault (DBF) on the west and east, respectively. DBF is considered as the boundary between the SSB and Central Iran (CI). Zagros Thrust Fault (the 'Zagros Thrust Line or ZTL in this study') also referred to as the 'Main Zagros Thrust', the 'Zagros suture' or the 'Main Zagros Reverse Fault' by various authors [e.g., 75,33,27,9] in the related articles, is shown to be deeply rooted and was the previous site of a paleotrench and could indicate position of the suture between the Iranian and Arabian Plates although its location has been doubted [e.g., 1,70, 4]. In this study, we investigate presence of the Zagros suture zone as a pre-existing major discontinuity [86,87] in a 3-D finite element model (TECTON 2.3 code) of [51,52] and its effect on the deformation history in the modeled area considering its proposed location [4,1] relative to the western boundary of the model. Based on the method introduced by [32] we simulate a zone of high strain localization corresponding to the suture. The results can be a support for observations that the suture zone could run most probably along the ZTL.

Regional Tectonic Elements

To satisfy the aims of this study that is: (1) to model numerically deformation pattern during time in the Eghlid-Deh Bid area and investigate the effects of a pre-existing discontinuity i.e., the Zagros suture on this pattern and, (2) to use the results to extend and generalize the model for the evolution of the Zagros suture zone, it will be necessary and reasonable to give a description of the evolution of regional tectonic elements around the study area with a brief explanation of the them. The study area, Eqhlid-Deh Bid Area (EDA) with an upside down triangular shape is located between 30°-31° latitudes and 52° 30 -54° longitudes (Fig. 1). It is bounded by Zagros Thrust Fault Line (ZTL) on the western edge (trending NW-SE) and by Deh Shir-Baft Fault (DBF) on the eastern edge (trending

nearly N-S), respectively. The upper third edge is a nearly E-W trending lineament [45,50]. According to [30] it appears that Eurasia has grown from the Middle to Late Triassic by successive accretion of micro-continents which came from the south, across the Tethyan seaway. The closure of Paleo-Tethys during Upper Permian–Late Triassic time resulted in welding of the existing micro-continents with the Eurasian Plate along a suture zone consisting of oceanic rocks. Nearly at the same time during the closure of Paleo-Tethys in the north, rifting along the present Zagros thrust zone of the continental plate took place, resulting in the opening of a new ocean called Neo-Tethys. With the disappearance of Paleotethys, the floor of Neo-Tethys started a north-dipping subduction beneath the Eurasian Plate during Triassic–Jurassic time. This caused a change in tectonic regime between the Arabian margin and the Iranian block from passive to convergent [30]. In this way, the Zagros orogen began to result from the convergence between the Iranian block and the Arabian Plate. Disappearance of the Neo-Tethyan realm was through a succession of subduction/obduction/collision stages [1]. During the Late Cretaceous, approximately 100-70 Ma ago [1], obduction occurred on the
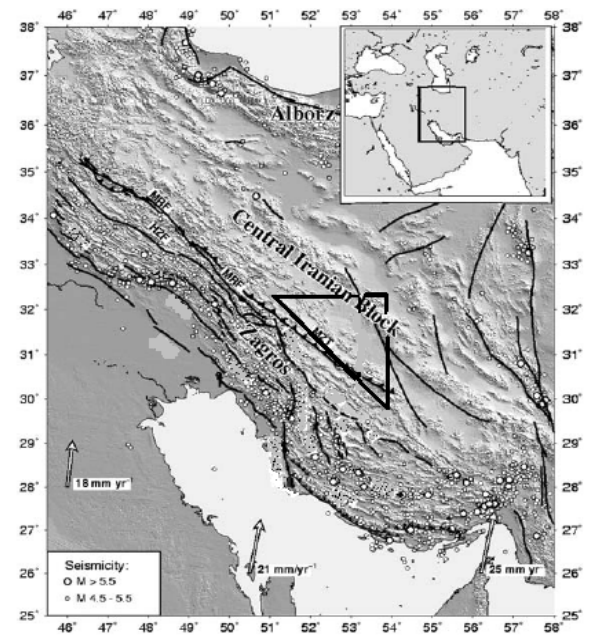

Figure 1. Location of the Zagros major active faults and seismicity and modeled area (triangle). The inset displays the global location of Zagros and Iran in the collision zone between the Arabian and Eurasian Plates. MRF: Main Recent Fault; MZT: Main Zagros Thrust; HZF: High Zagros Fault. After [9,22,89].

northeastern margins of the Arabian Plate. This obduction was caused by the convergence of the Iranian-Arabian plate [62,31,63] and led to an Early Cimmerian metamorphic event, recorded in the southwest of the SSB [10,11]. The final closure of Neo-Tethys and collision between the Arabian and Iranian Plates took place during the Neogene [10,12,30].

Numerical Modeling and Boundary Conditions

The main purpose of this article is to model the influence of a pre-existing discontinuity on deformation history and stress pattern in the modeled area. We used a 3D version of the finite element code, TECTON 2.3 [51,52]. The outputs were edited and displayed using Tecplot 10 software [80]. A total thickness of 100 km is given to the model domain comprising of three layers composing of the upper brittle and lower ductile crusts of the collided continent with a thickness of 20 and 40 km, respectively, and the lowest layer represents lithospheric mantle. The upper crust behaves as an elastic material (Table 1) while the lower crust is considered as a non-Newtonian viscous fluid layer with different power law exponent (n= 3, 5, 7) but the first one is included here as there wasn't any difference in the final patterns. The lithospheric mantle is taken as a low-viscosity material and is not allowed to move in any direction relative to the overlying layers. Here, a no-slip boundary condition along its base is applied [73]. An external boundary force equal to 3.55E+17 N [64] act normal to the western boundary which was resolved on the suture plane into suture parallel and normal components according to the angle of plate convergence as the only advancing boundary following a dynamic approach [64]. A time interval of 30 Myr [1,30,16] with time step of 30 to 150 was applied during each run. The eastern boundary (DBF) was allowed to slide in y-direction freely but the elements on its right side were fixed. The third side was allowed to move freely in x-direction. The Zagros suture zone was introduced as a high strain zone of localization [40,41] by defining a set of nodes [90] parallel to the ZTL. Two cases were examined: a marginal suture nearly at the place of the ZTL and, a median suture immediately behind the SSB (Fig. 2). Both cases have vertical dips in this study. The role of change in the suture plane dip is not considered here and will be presented in another paper. Displacement was fixed along z axis but allowable in x and y directions. The depth of the suture was limited to the depth of the lower crust as applied in the model, nearly coincident with theoretical seismogenic depths [18]. All of the boundaries have vertical dips regarding to theoretical basis and real field evidence [see for example; 40,47,54,88]. Two limitations of our modeling work are namely first, we didn't consider any thermal change from top to bottom of the model due to geothermal gradient and second, we couldn't apply split nodes in three dimensions to run the model in 3d mode.

Results

We present our modeling results in two parts regarding to the presumed position of the Zagros suture zone. The first part is devoted to the case in which a median suture zone immediately behind the SSB boundary [e.g., 2,4] is suggested (Fig. 2). The second part gives the results of the case where the Zagros suture is fixed at the position of the Zagros Thrust Line as a marginal suture [e.g., 1]. In both cases, the suture was allowed to slip along x and y axes without and movement along z axis. A combined presentation of contour lines and vectors were chosen to show simultaneously different and comparable features of the model results for example, displacement and stress values and their variation from top to bottom of the model.

Median Suture Zone

Regarding to width of the study area (approximately 200 km) a median suture was located nearly at the middle of the model running parallel to the ZTL trend. The length of the selected suture was so that it didn't interact with other boundaries of the model. As noted previously for the other boundaries, here a vertical dip was also attributed to the specified suture.

Table 1. Summary of mechanical parameters used in the numerical modeling

Name	Symbol	Unit	Value
Young's modulus	c	Pa	1.00E+11
Poisson's ratio			0.25
Density	ρ	Kg/m³	2.70e3 (upper crust)
	ρ	Kg/m³	2.80e3 (lower crust)
	ρ	Kg/m³	3.00e3 (upper mantle)
Viscosity coefficient		Pa	1.00E+11
Power law			1.0 (upper crust)
			3.0 (lower crust)
Cohesion	c	Pa	1.00E+07
Friction angle	φ		30

Displacement Field Pattern

    Figures 3 and 4 show displacement field pattern and its variation for different components in the study area. Displacement are given in Km. Each component is plotted as contour lines but total displacement is shown as vector. Figure 3 shows displacement components along x and y directions and their relative change with depth. Cross sections are along the top and bottom of the model. As shown, a clear separation is happened between displacement vectors along the suture zone. The nearly straight shape of the displacement contours parallel to the suture zone is visible on the model surface. Of course, the pattern is different from top to bottom of the model mainly due to downward extension of the suture i.e., its limitation to the crust thickness. The displacement pattern in both directions behind the suture line is almost uniform and its magnitude is constant but less than that seen on the left side of the suture (Fig. 3). This pattern is also seen for z-direction but the amount of displacement is larger is behind the suture line (Fig. 4). A clear difference between x and y-components from z component is that the displacement pattern does not change with depth for the z component. The general pattern of the displacement field resulted from our modeling is shown in Figure 5.

Stress Field Pattern

    To show the role of a suture zone as the representative of a pre-existing discontinuity in the study area, different components of the stress field and their variation with depth during time period are given in a block diagram set presented in Figure 6. The variation of Sxx and Syy (in MPa) versus depth is shown in Figure 6a and b. Shear stress components (Sxy and Syz) and their pattern change versus depth is illustrated in Figure 6c and d. The elongated shape of normal stress pattern (Fig. 6a and b) is affected by the position of the median suture and is restricted to southwestern side of the suture. The amount of Sxx increases northward whereas it is southward for Syy. The amount of the stress increases from top to bottom of the model partly because the lower layer of the model i.e., lithospheric mantle was fixed and not allowed to move relative to the upper layers. As the effect of the suture was more clearly observed in shear stress components, it was preferred to present their pattern as vector diagram. Figure 6 (c and d) compare such an effect for Sxy and Syz shear stresses, respectively. Since, the pattern for Szx is almost the same as for Sxy, we didn't show it. As can be seen, the presence of the suture divides the region into two parts; the direction of vectors is from east to west to the left side of the suture but it is reversed to the right of the suture (Fig. 6c and

d). Additionally, an NE-SW break is seen for Syz plot (Fig. 6d) below the location of the suture. The shear stress direction is uniformly toward east to the right of suture for Syz. Additionally, an NE-SW break is seen for Syz plot (Fig. 6d) below the location of the suture. The shear stress direction is uniformly toward east to the right of suture for Syz. Such a pattern forces one to imagine an extensional zone at the suture which is not in accordance with the existing evidence. The problem is more debating for the case of Figure 6d.

Marginal Suture Zone

    The location of marginal suture was fixed nearly at the place of the ZTL. To prevent calculation errors due to the elements geometry, the suture was located at the nodes immediately after those defining the ZTL. The applied geometry and boundary conditions is similar to those of a median suture explained in Section 1.

Displacement Field Pattern

    Displacement field pattern and its variations for different components in the study area are shown in Figures 7 and 8. Each displacement component is plotted as contour lines but total displacement is shown as vector. Figures 7a and 7b show displacement components along x and y directions and their relative change with depth. Cross sections are again along the top and bottom of the model. The maximum amount of displacement (contours) in Km is toward NW and SE for x and y components, respectively. However, the pattern is almost uniform for the bottom layer and shows a southward increase. As illustrated, a semi uniform displacement direction is located at the place of the suture zone on the upper cross sections ((Fig. 7a and 7b). It also depicts a moderate elongation parallel to the suture line. The overall shape of the displacement contours indicates an elongation parallel to the suture zone. The effect of the suggested suture is more obvious for displacement component along z axis (Fig. 8). Here, a distinct downward displacement can be seen behind the suture line and inside the model boundaries. The general pattern of the displacement field form top to the bottom of the model is shown in Figure 9.

Stress Field Pattern

    The pattern of stress field for normal and shear components are given in Figure 10. Figure 10a and b are block diagrams of the normal components Sxx and Syy, respectively. The position of the suture is appeared as a clear cut in the contours pattern. The pattern indicates a northward and southward increase for Sxx Syy, respectively. Thus, the suture bears less effect in regions
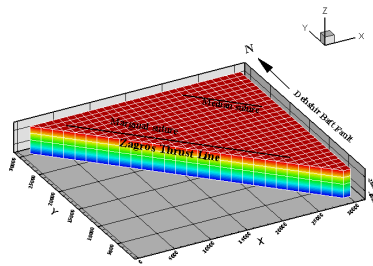
Figure 2. Three dimensional mesh (200*200 km) plot of the study area. Zagros Thrust Line shows general location of this fault. The two black lines indicate located positions of Zagros suture line for two different cases considered in the model.
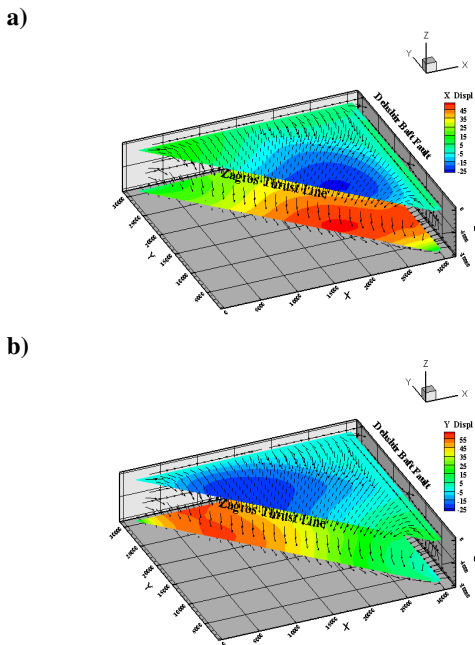
a)

b)

Figure 3. Cross sections of displacement field for x (a) and y (b) components and their variation on the top and bottom of the model. Vectors show variation of the total displacement. Zagros Thrust Line shows general location of this fault.

a)

b)

Figure 4. Cross section and block diagram of the displacement component Z. Vectors show total displacement change form top to bottom of the model. The location of the suture in this case is shown as a red bold line.

Figure 5. General pattern of the displacement field and its downward variation. Zagros Thrust Line shows general location of this fault. Depth scale (Z) is in m *10.

where sense of fault movements is similar. As for the median suture, a downward increase is seen in the amount of the stress. The effect of the suture on shear stress components is presented in Figure 10c and d. As shown, the presence of the suture is very significant at its position and a triangular zone has been formed in the middle of the model. The general direction of vectors demonstrates a clockwise rotational pattern which is clearer for Sxy component (Fig. 10c). The shape of the
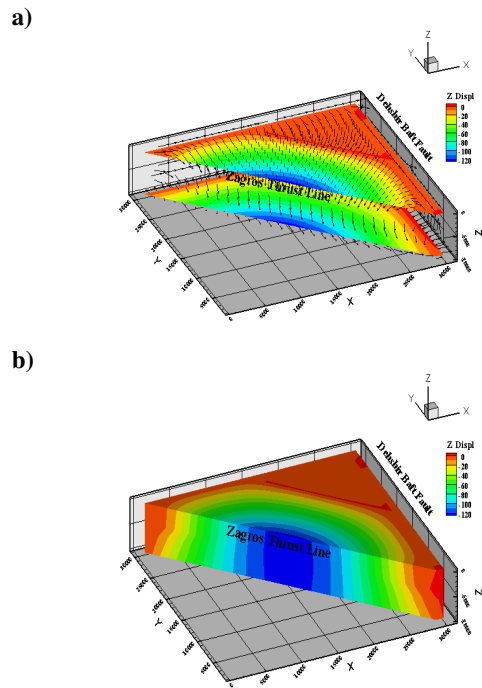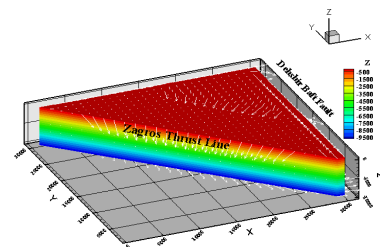
vector pattern at the ZTL is highly affected by the boundary conditions because we applied the driving force normal to the western side and did not allow the suture to move laterally but only in the z direction. The direction of Szx vectors reveals a downward shape in the middle part of the region (Fig. 10d) while it is nearly upward at the corners. This pattern is in agreement with general topography of the study area (Figs. 2 and 16, Arzani 2005).
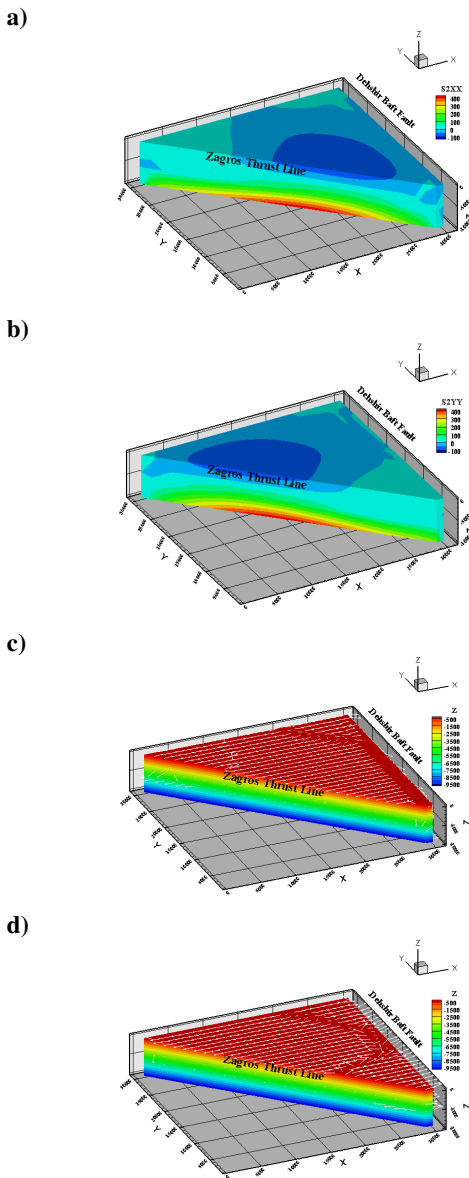
a)

b)

c)

d)

Figure 6. Stress components (Sxx, Syy, Sxy, Syz) variations, respectively for the study area. Zagros Thrust Line shows general location of this fault. See text for details. Depth scale (Z) in c and d is in m *10.

a)

b)

Figure 7. Cross sections of displacement field for x (a) and y (b) components and their variation on the top and bottom of the model. Vectors show variation of the total displacement. Zagros Thrust Line shows general location of this fault.

Discussion

Regarding to the above mentioned results of the present study, we will present some more block diagrams containing extra evidence to distinguish between median and marginal suture zones effects on the deformation pattern in the study area and their
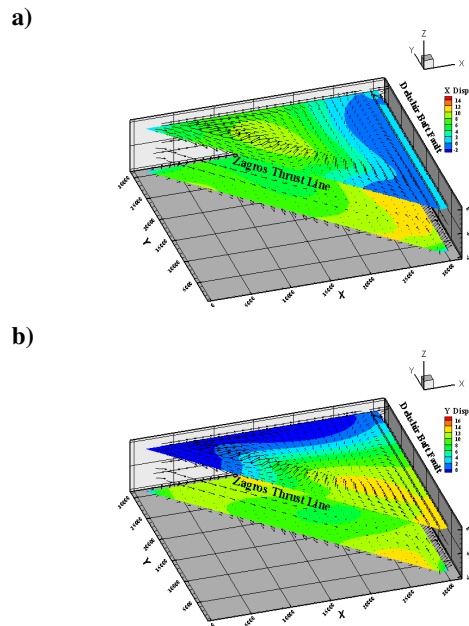
similarities and contrasts with plate scale shear zones. Also, we will discuss their possible explanations according to the existing theoretical and experimental issues or field observations. Here, we try to present as much as possible satisfying and reasonable evidence to improve our discussions and conclusions.

Median Suture Zone

Figure 11 shows downward variation (contours) of the more sensible stress components i.e., Sxy and Szx in the top and bottom cross sections of the modeled area for two successive runs. Embedded in the cross sections are vectors depicting displacement changes. The Sxy is almost uniform on the northeast of the median suture but shows a concentration on the northwest of it (Fig. 11a and b). The suture divided the area into two parts regarding to the displacement vectors (upper sections in the Fig. 11). The direction of the vectors is nearly NE to SW on the right side of the suture but is downward on its left side. The amount of the displacement increases towards west i.e., the ZTL as mentioned in the previous sections. Figures 11 c and d give the results for Szx. Here, the stress field is separated into banded zones on the right side of the suture. However, it gradually

becomes uniform throughout the region in successive time steps (Fig. 11c and d, respectively). Additionally, it shows a triangular pattern on the bottom section which increases inward.

Marginal Suture Zone

The effect of the marginal suture on the pattern of stress and displacement fields is illustrated in Figures 12a to 12d. As shown, the stress component (Sxy) is localized along the suture colored in grass green (Fig. 12a and b) with a southward necking parallel with the ZTL. This pattern is nearly repeated for the Szx (Fig. 12c). The displacement vectors are nearly tangential at the ZTL and towards NE at the suture zone.

The stress pattern for the Szx component on the bottom sections (Fig. 12c and d) is similar to that of the median suture with the same variations. Similarly, a gradual uniformity of the Szx is gained through the successive time steps for the whole region (Figure 12c and d, respectively). Regarding to the above results and referring to the existing literature about shear zones geometry and behavior particularly at plate boundary scale, the evidence gathered here are mostly consistent with the effects of a marginal suture zone on the deformation pattern and history in the study area i.e., Eghlid-Deh Bid which cab extended to nearly whole of the Zagros Fold-Thrust Belt (ZFTB). To reinforce our conclusions we check the model by inserting some additional boundary conditions relative to the applied suture zone. These requisites include allowing the suture to slip laterally along x and y axes and to observe displacement changes during successive times steps. We didn't present the resulting displacement along the x axis as it was not very obvious and significant. Figure 13 illustrates the effect of motion along the median (a) and marginal (b) sutures at the end of a three step running procedure. As can be seen, the median suture didn't make a simply differentiable partitioning on its sides while such a separation is very clear for the case of marginal suture. This pattern coincides with reported right lateral movement along the ZTL at its north-western continuation. Besides, the expected amount of this strike-slip motion increases southward which is consistent with the above mentioned results. It also depicts a linear localization of displacement which is theoretically in agreement with previous studies of large scale shear zones [e.g., 28, 56]. In a similar way we ran the model with a marginal suture zone and saw the pattern of displacement during a 30Ma time period (Fig. 14).

As shown, the resulted pattern is very consistent and in good agreement with present shape of the study area and the observed deformation patterns [65,66]. Although, the displacement is highly concentrated along the ZTL (Fig. 14a) but it gradually spreads over the region (Fig. 14c). They are comparable with the observed phases of deformation in the area [67], as well. The final resulted pattern is also confirmed by previous analogue modeling [15]. Accordingly, as an opportunity has been available by the Iranian-Arabian continental collision (i.e., Eghlid-Deh Bid area as part of it) to
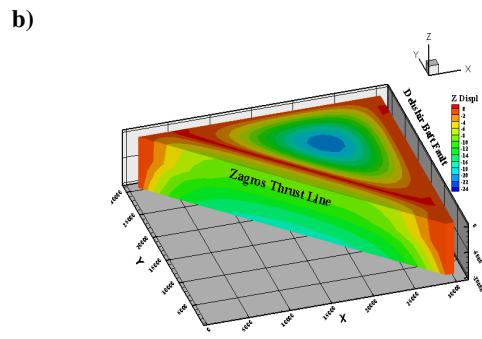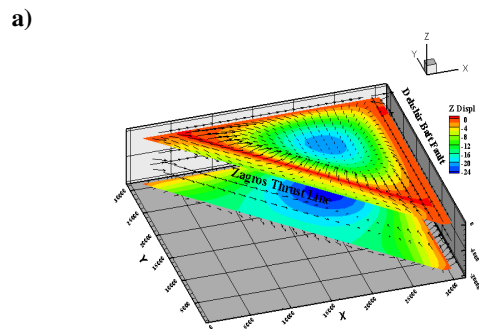
a)

b)

Figure 8. Cross section and block diagram of the displacement component Z. Vectors show total displacement change form top to bottom of the model. The location of the suture in this case is shown as a bold red line.
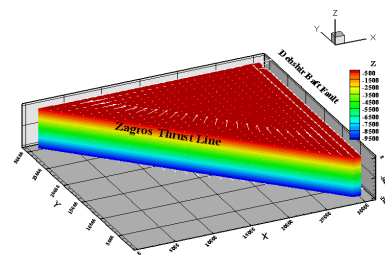

Figure 9. General pattern of the displacement field and its downward variation. Zagros Thrust Line shows general location of this fault. Depth scale (Z) is in m *10.
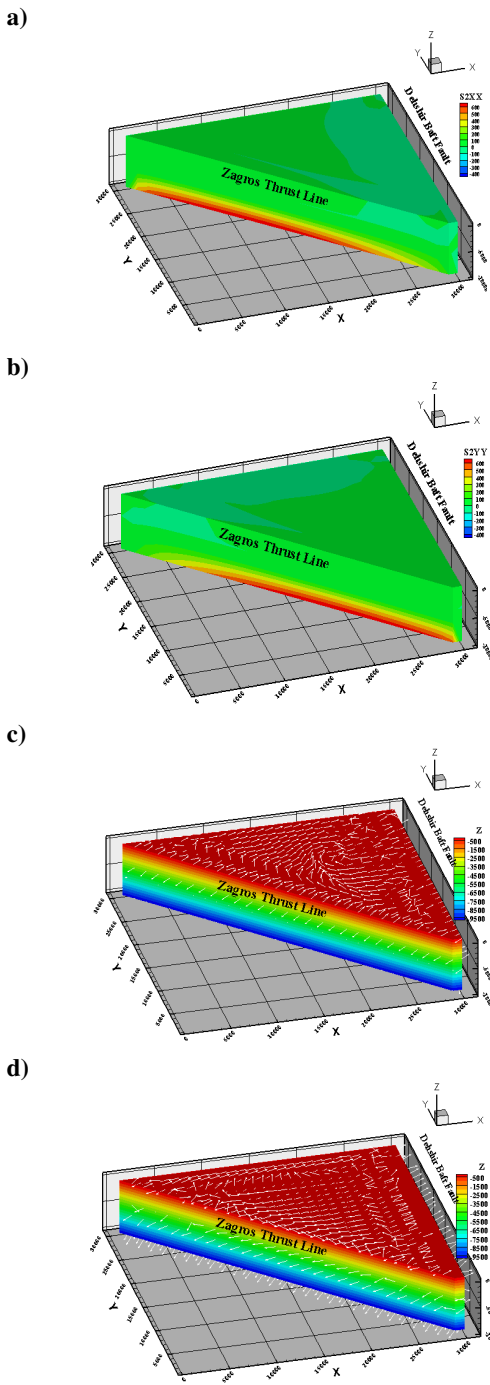
a)

b)

c)

d)

a)

b)

c)

d)

Figure 10. Stress components (Sxx, Syy, Sxy, Szx) variations, respectively for the study area. Zagros Thrust Line shows general location of this fault. Depth scale (Z) in c and d is in m *10. See text for details.
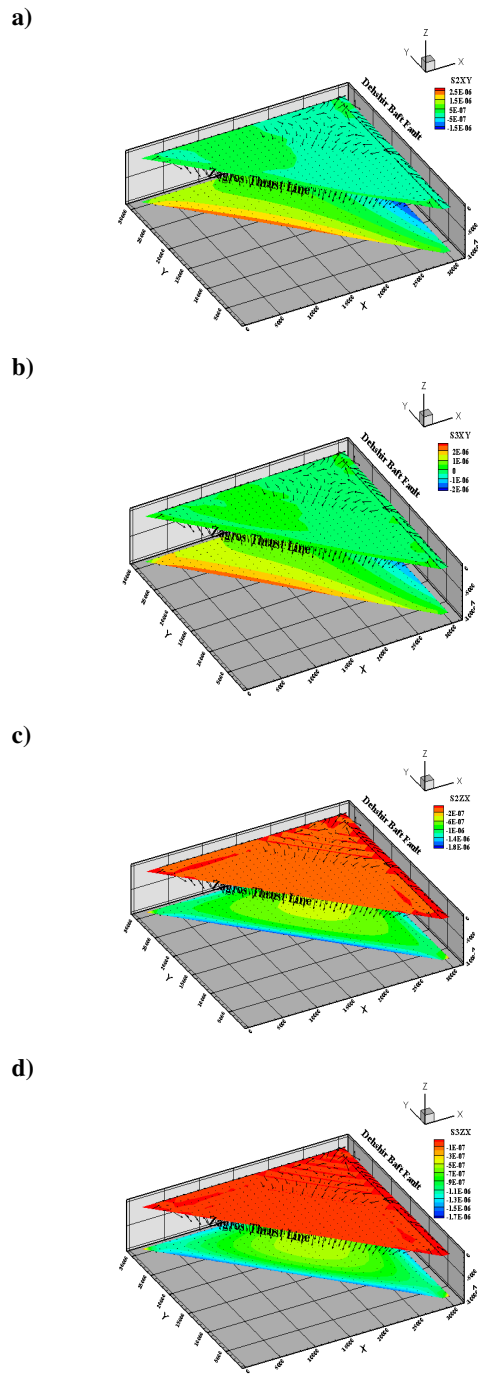
Figure 11. General displacement field (vectors) added to downward variation of the stress components (Sxy, Szx) shown as contours resulted from a median suture in the study area. Zagros Thrust Line shows general location of this fault. See text for details.
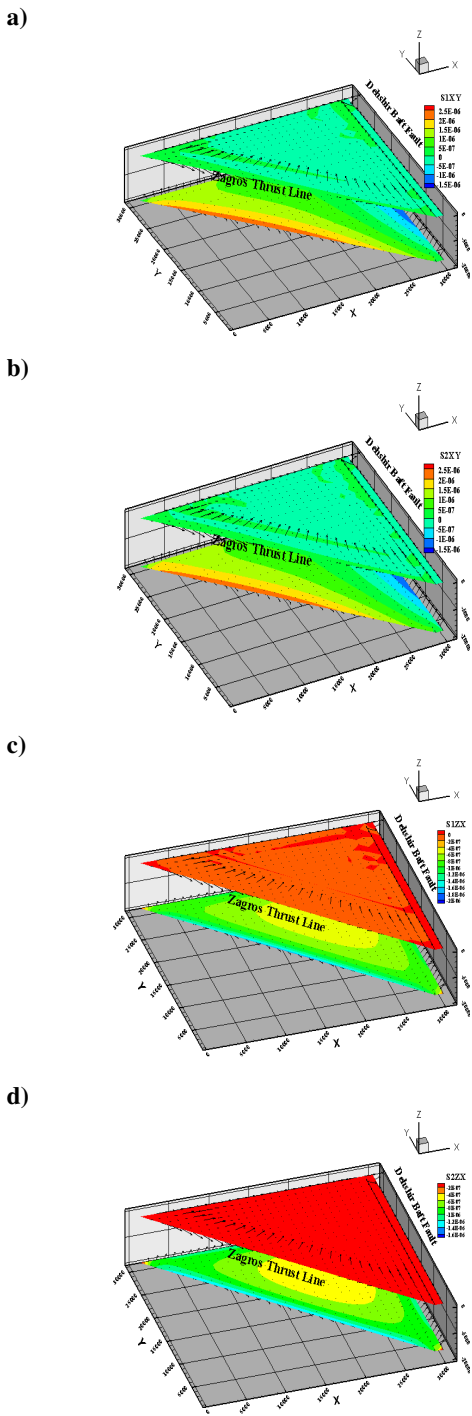
a)

b)

c)

d)

better understand strain localization along major fault systems of continental crust, we can develop our model findings to the ZFTB as a plate scale shear zone. The direction of displacement vectors, their pattern and variation from surface to depth are in good agreement with oblique relative motion at convergent plate margins which is an inevitable consequence of the progressive movement of plates on the surface of a sphere [21,93]. The pattern of stress components and their changes with depth in addition to their partitioning into separate sub-zones may be an indication of non-coaxial non-plane strains which partly have been approved by primary microstructural measurements in the field [67]. Finally, the model results predicted a dextral wrenching along the ZTL. It should be reminded that the force was applied normal to the western side of the model but resolved into components onto the plane of the suture. This could confirm rearrangement of the tectonic environment during time span and its gradual change from nearly pure compression into dextral transpression. Such a model is a proof for the fact that the separation of Arabia from the African Plate and its subsequent collision with Eurasia was the last of a series of separation/collision events combining the extensive

a)

b)

Figure 12. General displacement field (vectors) added to downward variation of the stress components (Sxy, Szx) shown as contours resulted from a marginal suture in the study area. Zagros Thrust Line shows general location of this fault. See text for details.
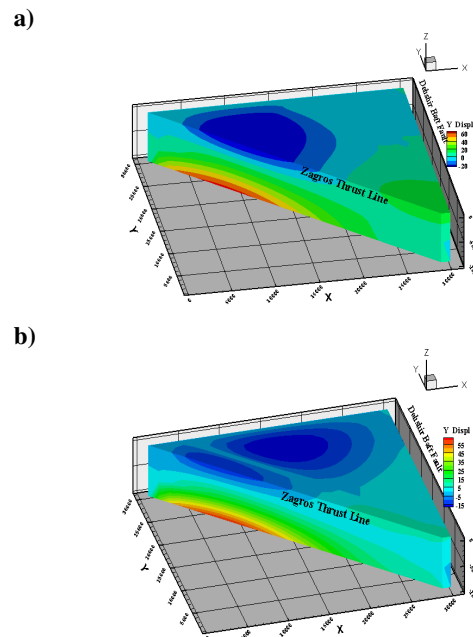
Figure 13. General displacement field resulted from strike-slip motion along median (a) and marginal (b) sutures for the study area. Zagros Thrust Line shows general location of this fault.
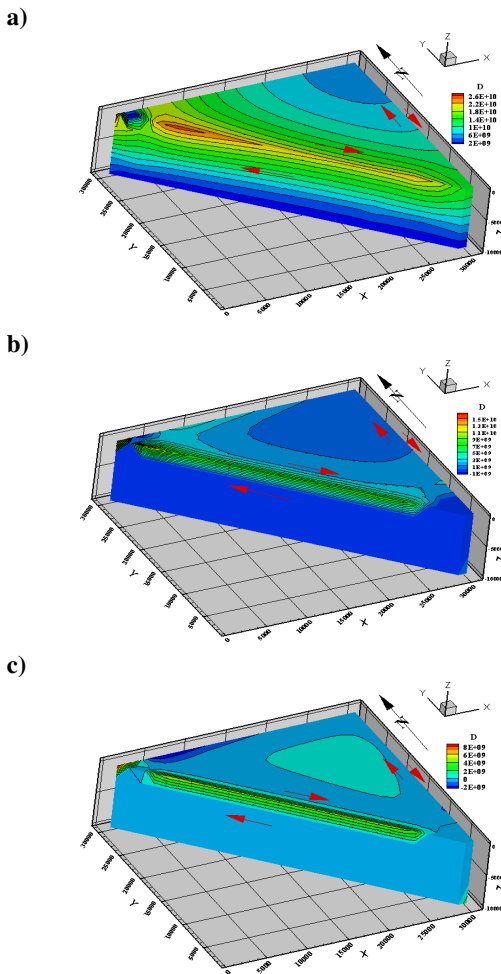
a)

b)

c)

Figure 14. Displacement field resulted from the marginal suture zone at the beginning, middle and end of a sample run with a time period of 30Ma.

Alpine and Himalayan orogenic system. Finally, the main conclusions of the present study can be summarized as follows: numerical modeling of Eghlid-Deh Bid area as part of the ZFTB which is in turn a manifestation of the Iranian-Arabian continental collision reveals some information about regional deformation pattern and role of a pre-existing discontinuity i.e., the Zagros suture zone, on the pattern of displacement and stress fields in the study area. As the study area is mostly composed of SSB, the obtained results can be compared and partly confirmed by some limited structural and microstructural data gathered by other researchers.
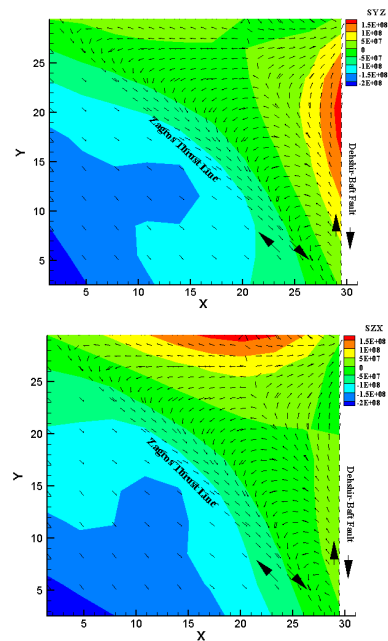

Figure 15. A synoptic plot of Sxy/Syz ratio (vectors) in the y-z (a) and z-x (b) sections, respectively. The lower left sides of the plots have been simulated by Tecplot 10.

Based on the modeling results, subdivision of the area into smaller parts due to the presence of a suture zone regarding to the width of the SSB, topography and structural or microstructural evidence is mostly consistent with a marginal suture located nearly at the place of the ZTL [e.g., 1] and a distant suture i.e., behind the boundary limit of the SSB, for example at the middle distance between the ZTL and DBF, would not result in stress and displacement patterns fairly reasonable and approvable especially by previous field surveys. The overall stress and displacement patterns obtained from our model are in good agreement with those of common non-coaxial shear zones formed at plate boundaries [e.g., 40,41]. They are also supported by previous modeling works [e.g., 15]. The results show that the stress components are mainly concentrated at the model boundaries which are defined by major structural features such as the Zagros thrust fault, the Zagros suture and DBF. Besides, they increase toward the junction of structural trends. The results also indicate gradual rearrangement of displacement and stress pattern during time span that change tectonic environment from almost pure compressional to oblique transpressional regime. Such a transformation of tectonic regime is theoretically coherent with intrinsic

progressive movement of plates on the surface of a sphere although, some limited field data confirm these changes [65,66,67]. It also could be a product of indentation tectonics [e.g., 39,42,48,49,60,73] but has not been investigated here although some of the results are possibly indicative of such a phenomenon (Fig. 15). However, it would remain to be a subject of the future research.

Acknowledgements

References

1. Agard, P., Omrani, J., Jolivet, L., and Mouthereau, F. Convergence history across Zagros (Iran): constraints from collisional and earlier deformation. Int J Earth Sci (Geol Rundsch) **94**: 401–419 (2005).

2. Alavi, M. Regional stratigraphy of the Zagros fold-thrust belt of Iran and its pro-foreland evolution: American J. Science, vol. **304**, p. 1–20 (2004).

3. Alavi, M., Vaziri, H., Seyed-Emami, K., Lasemi, Y. Triasic and associated rocks of the Nakhlak and Aghdarband areas in central and northeastern Iran as remnant of the southern Turanian active continental margin. Geological Society of America Bulletin **109**, 1563-1575 (1997).

4. Alavi, M. Tectonics of the Zagros orogenic belt of Iran: new data and interpretations: Tectonophysics, v. **229**, p. 211–238 (1994).

5. Allen, M., Jackson, J., and Walker, R. Late Cenozoic reorganization of the Arabia-Eurasia collision and the comparison of short-term and long-term deformation rates. TECTONICS, vol. **23**, TC2008, doi: 10.1029/ 2003TC001530 (2004).

6. Ambraseys, N. & Jackson, J. Faulting associated with historical and recent earthquakes in the Eastern Mediterranean region, Geophys. J. Int., **133**, 390–406 (1998).

7. Ambraseys, N. & Melville, C. A history of Persian earthquakes, Cambridge University Press, Cambridge. UK, (1982).

8. Arzani, N. The fluvial megafan of Abarkoh Basin (Central Iran): an example of flash-flood sedimentation in arid lands In: Harvey, A.M., Mather, A.E. and Stokes, M. (eds). Alluvial Fans: Geomorphology, Sedimentology, Dynamics. Geological Society, London, Special Publications. **251**, 41–59 (2005).

9. Berberian, M. Master blind thrust faults hidden under the Zagros folds: active basement tectonics and surface morphotectonics. Tectonophysics, **241**, 193–224, (1995).

10. Berberian, F., Berberian, M. Tectono-plutonic episodes in Iran. In: Gupta, H.K., Delany, F.M. (Eds.), Zagros, Hindu Kush, Himalaya. Geodynamic Evolution, American Geophysical Union, Geodynamics Series **3,** pp. 5–32 (1981).

11. Berberian, M. and King, G.C.P. Towards a Paleo-geography and Tectonics Evolution of Iran, Can. J.Earth Sci., **18**, 210-265 (1981).

12. Berberian, F., Muir, I.D., Pankhurst, R.J., Berberian, M. Late Cretaceous and early Miocene Andean-type plutonic activity in northern Makran and Central Iran. Journal of the Geological Society of London **139,** 605–614, (1982).

13. Bird, P. Finite element modeling of lithosphere defor-mation: the Zagros collision orogeny, Tectonophysics, **50**, 307–336 (1978).

14. Bird, P., Piper, K. Plane-stress finite-element models of tectonic flow in southern California. Physics of Earth and Planetary Interiors **21**, 158-175 (1980).

15. Bonini, M., et al. Insights from scaled analogue modelling into the Seismotectonics of the Iranian region. Tectonophysics, v**. 376**, p. 137–149 (2003).

16. Boulin, J. Structures in Southwest Asia and evolution of the eastern Tethys. Tectonophysics **196**, 211–268 (1991).

17. Buck, W.R., Poliakov, A.N.B. Abyssal hills formed by stretching oceanic lithosphere. Nature **392**, 272– 275 (1998).

18. Byerlee, J. Friction of Rocks. Pure and Applied Geophysics, vol. **116**, p. 615-626 (1978).

19. Dehghani, G.A. and Makris, J. The gravity field and crustal structure of Iran. N. Jb. Geol. Pal¨aont. Abh**., 168**, 215–229 (1984).

20. DeMets, C., Gordon, R. G., Argus, D. F. and Stein, S. Current plate motions. Geophysical Journal International, vol. **101**, p. 425-478 (1990).

21. Dewey, J.F. Finite plate evolution: some implications for the evolution of rock masses at plate margins. American Journal of Science**, 275**, 260–284 (1975).

22. Engdahl, E.R., Van der Hilst, R.D. and Buland, R.P. Global teleseismic earthquake relocation with improved travel times and procedures for depth determination, Bull. Seism. Soc. Am**., 88**, 722–743 (1998).

23. England, P.C., Houseman, G.A. Finite strain calculations of continental deformation. 2: comparison with the India-Asia collision zone. Journal of Geophysical Research, **91** (B3), 3664-3676, (1986).

24. England, P. and McKenzie, D.P. A thin viscous sheet model for continental deformation, Geophys.J. Roy Astr. Soc., **70**, 295-321, (1982).

25. England, P. and McKenzie, D.P. Correction to: a thin viscous sheet model for continental deformation, Geophys. J. Roy Astr. Soc**., 73**, 523-532, (1983).

26. Faccenna, C., Davy, P., Brun, J.P., Funiciello, R., Giardini, D., Mattei, M.,and Nalpas, T. The dynamic of backarc basins: an experimental approach to the opening of the Tyrrhenian Sea. Geophysical Journal International **126**, 781– 795, (1996).

27. Falcon, N.L. Southern Iran: Zagros Mountains, Spencer (Editor), Mesozoeic-Cenozoice Orogenic Belts, and Data for Orogenic Studies, Geol. Soc. London, Spec. Publ., **4,** 199-211 (1974).

28. Fitch, T. J. Plate convergence, transcurrent faults, and

internal deformation adjacent to South East Asia and the western Pacific. J. Geophys. Res**., 77**, 4432 (1972).

29. Ghazi, A.M., Hassanipak, A.A., Mahoney, J.J., and Duncan, R.A. Geochemical characteristics, 40Ar–39Ar ages and original tectonic setting of the Band-e-Zeyarat/Dar Anar ophiolite, Makran accretionary prism, S.E. Iran. Tectonophysics, **393,** 175– 196, (2004).

30. Golonka, J. Plate tectonic evolution of the southern margin of Eurasia in the Mesozoic and Cenozoic. Tectonophysics, **381**, pp.235– 273, (2004).

31. Guiraud, R., Bellion, Y. Late Carboniferous to recent geodynamic evolution of the west Gondwanian Cratonic Tethyan margin. In: Nairn, A.E.M., Ricou, L.-E., Vrielynck, B., Dercourt, J. (Eds.), The Oceans Basins and Margin. The Tethys Ocean, vol**. 8.** Plenum, New York, pp. 101–124, (1996).

32. Hall-Wallace, M., and Melosh, H.J. Buckling of a pervasively faulted lithosphere. PAGEOPH, Vol. **142,** No. 2. 239-261, (1994).

33. Haynes, S.L., and McQuillan, H. Evolution of the Zagros suture zone, Southern Iran .Geol .Soc.Am.Bull.**85**, 739– 744, (1974).

34. Hochstein, M.P., and Regenauer-Lieb, K. Heat generation associated with the collision of two plates: the Himalaya Geothermal Belt. Journal of Volcanology and Geothermal Research **83** (1–2), 75– 92, (1998).

35. Houseman, G., and England, P.C. Finite strain calculations of continental deformation. 1: method and general results for convergent zones. Journal of Geophysical Research **91,** (1986).

36. Houshmandzadeh, A.R., Ohanian, T., Sahandi, M.R., Taraz, H., Aganabati, A., Soheili, M., Azarm, F.,and Hamdi, B. Geological map of Eglid Quadrangle G10. 1: 250000, Geological Survey of Iran, Tehran, Iran, (1975).

37. Jackson, J., Haines, J. and Holt, W. The accommodation of Arbia-Eurasia plate convergence in Iran. J. Geophys. Research, vol**. 100**, p. 15,205-15,219, (1995).

38. Jackson, J.A., and McKenzie, D.P. Active tectonics of the Alpine-Himalayan Belt between western Turkey and Pakistan. Geophys. J. of the Royal Astronomical Society **77**, 185–264, (1984).

39. Jeˇzek, J., Schulmann, K., and Thompson, A.B. Strain partitioning in front of an obliquely convergent indenter. EGU Stephan Mueller Special Publication Series, 1, 93– 104, (2002).

40. Jiang, D., Lin, S., and Williams, P.F. Deformation path in high strain zones, with reference to slip partitioning in transpressional plate-boundary regions. J.Struct.Geol**., 23**, 991-1005 (2001).

41. Jones, R.R., Holdsworth, R.E., McCaffrey, K.J.W., Clegg, P.,and Tavarnelli, E. Scale dependence, strain compatibility and heterogeneity of three-dimensional deformation during mountain building: a discussion. J. Struct. Geol., **27**, 1190-1204 (2005).

42. Kadinsky-Kade, K., and Barazangi, M. Seismotectonics of southern Iran: The Oman line. Tectonics, v.**1,** No.5, p. 389-412, (1982).

43. Kaviani, A. La chaıne de collision continentale du Zagros (Iran): structure lithosph´erique par analyse de donn´ees sismologiques. Observatoiredes Sciences de l'Univers de Grenoble. Grenoble, Universit´e Joseph Fourier**: 228,**

(2004).

44. Kreemer, C., W. E. Holt, and Haines, A. J. An integrated global model of plate motions and plate boundary deformation. Geophys. J. Int**., 154**: present-day 8–34 (2003).

45. Kronberg, P. Patterns and principles of crustal fracturing as deduced from a Landsat-mosaic covering central and eastern Iran: GSI, Report no. **51**, p.37-50 (1983).

46. Masson, F., Ch´ery, J., Hatzfeld, D., Martinod, J., Vernant, P., Tavakoli, F. and Ghafori-Ashtiany, M. Seismic versus aseismic deformation in Iran inferred from earthquakes and geodetic data. Geophys. J. Int**., 160**, 217–226 (2005).

47. McKenzie D., and Jackson, J. The relationship between strain rates, crustal thickening, palaeomagnetism, finite strain and fault movements within a deforming zone. Earth and Planetary Science Letters**, 65**, 182-202 (1983).

48. McQuarrie, N. Crustal scale geometry of the Zagros fold thrust belt Iran. J Struct Geol **26**:519–535 (2004).

49. McQuarrie, N., J. M. Stock, C. Verdel, and Wernicke, B. P. Cenozoic evolution of Neotethys and implications for the causes of plate motions, Geophys. Res. Lett., **30**, 2036, doi: 10.1029/ 2003GL017992 (2003).

50. McQuilan, H. The role of basement tectonics in the control of sedimentary facies, structural patterns and salt emplacement in the Zagros fold belt of southwest Iran, J. Southwest Asian Earth Sci., vol. **5.**, Nos. 1-4, pp. 453-463 (1991).

51. Melosh, H. J., and Raefsky, A. The Dynamical Origin of Subduction Zone Topography, Geophys. J. R. A. S**. 60,** 333-354 (1980).

52. Melosh, H. J., and Williams, C. A. Mechanics of Graben Formation in Crustal Rocks: A Finite Element Analysis, J. Geophys. Res**. 94,** 13961-13973 (1989).

53. Meyer, B., F. Mouthereau, O. Lacombe and Agard, P. Evidence of Quaternary activity along the Deshir Fault: implication for the Tertiary tectonics of Central Iran, Geophys. J. Int**. 164,** 192–201 (2006).

54. Mohajjel, M., and Fergusson, C. Dextral transpression in Late Cretaceous continental Collision zone, western Iran: J. Struct. Geol., v. **22**, p.1125–1139 (2000).

55. Mohajjel M, Fergusson CL, and Sahandi M.R. Cretaceous–Tertiary convergence and continental collision Sanandaj–Sirjan zone, Western. Iran. J Asian Earth Sci**., 21,** p.397–412 (2003).

56. Molnar, P. Brace-Goetze strength profiles, the partitioning of strike-slip and thrust faulting at zones of oblique convergence and the stress-heat flow paradox of the San Andreas fault. In: Evans, B., Wong, T. (Eds.). Fault Mechanics and Transport Properties of Rocks. Academic Press, San Diego pp. 435-459 (1992).

57. Ni, J. and Barazangi, M. Seismotectonics of the Zagros continental collision and comparison with the Himalayas. J. geophys. Res**., 91**, 8205–8218 (1986).

58. Nogole-Sadate, M.A.A. Les zones de decrochement et les virgations structurales en Iran. Geol. Survey. Iran. Report 55, (1985).

59. Paul, A., Kaviani, A., Hatzfeld, D., Vergne, J., and Mokhtari, M. Seismological evidence for crustal-scale thrusting in the Zagros mountain belt (Iran). Geophys. J. Int. doi: **10.1111**/j.1365-246X.2006.02920.x (2006).

60. Regard, V., Faccenna, C., Martinod, J., and Belliera, O.

Slab pull and indentation tectonics: insights from 3D laboratory experiments. Physics of the Earth and Planetary Interiors**, 149**, 99–113 (2005).

61. Reinecker, J., O. Heidbach, and Mueller, B. The 2003 release of the World Stress Map. Available online at www. world-stress- map.org (2003).

62. Ricou, L.-E. The plate tectonic history of the past Tethys Ocean. In: Nairn, A.E.M., Ricou, L.-E., Vrielynck, B., Dercourt J. (Eds.). The Oceans Basins and Margin. The Tethys Ocean, vol. **8**. Plenum Press, New York, pp. 3-70 (1996).

63. Robertson, A.H.F., and Searle, M.P. The northern Oman Tethyan continental margin: stratigraphy, structure, concepts and controversies. In: Robertson, A.H.F., Searle, M.P., Ries, A.C. (Eds.). The Geology and Tectonics of the Oman Region. Special Publication-Geological Society, vol**. 49**, pp. 3-25 (1990).

64. Sargent, M.T. Dynamics of the Eurasian Plate, Ph.D. thesis, Swiss Federal Institute of Technology Zurich ,81p, (2004).

65. Sarkarinejad, K. Structures and microstructures related to steady-state mantle flow in the Neyriz ophiolite, Iran. J. Asian Earth Sci**., 25**, p.859–881 (2005).

66. Sarkarinejad, K. Structural and microstructural analysis of a palaeo-transform fault zone in the Neyriz ophiolite, Iran, in: Dilek, Y., and Robinson, P.T., (eds). Ophiolites in Earth History. Geol. Soc. London, Spec. Publ., **218**, p. 129-145 (2003).

67. Sarkarinejad, K., Heyhat, M. R., and Faghih, A. Deformation conditions, Kinematics, and displacement history in Dehbid Shear Zones, Iran. Geophysical Research Abstracts, Vol. **9,** 00716 (2007).

68. Schreurs, G. Fault development and interaction in distributed strike-slip shear zones: an experimental approach. Geological Society, London, Special Publications; v**. 210**; p. 35-52, (2003).

69. Searle, M.P. Cooling history, exhumation and kinematics of the Himalaya-Karakorum–Tibet orogenic belt. In: Yin, An and Harrison, T.M. (Eds.), The Tectonic Evolution of Asia. Cambridge Univ. Press, Cambridge, pp. 110-137 (1996).

70. Shahidi, M and Nazari, H. Geological map of Harsin, 1/100.000 scale. Geological survey of Iran, (1997).

71. Shemenda, A.I., and Grocholsky, A.L. Physical modeling of slow seafloor spreading. Journal of Geophysical Research **99 (B5),** 9137– 9153 (1994).

72. Sobouti, F., and Arkani-Hamed, J. Numerical modelling of the deformation of the Iranian plateau, Geophys. J. Int., **126**, 805-818 (1996).

73. Sokoutis, D. et al. Indentation of a continent with a built-in thickness change: experiment and nature, Tectonophysics, v. **320**, p. 243–270 (2000).

74. Soofi, M.A. and King, S.D. Oblique convergence between India and Eurasia, J. Geophys. Research, VOL. **107,** NO. B5, 10.1029/2001JB000636 (2002).

75. Stocklin, J. Structural history and tectonics of Iran: a review: A.A.P.G., Bulletin, v. **52**, p. 1229–1258 (1968a).

76. Talebian, M., and Jackson, J. Offset on the Main Recent Fault of NW Iran and implications for the late Cenozoic tectonics of the Arabia-Eurasia collision zone, Geophys. J. Int**., 150,** 422 – 439 (2002).

77. Taraz, H. Geology of the Surmagh-Deh Bid area, Abadeh region, central Iran: Geological Survey of Iran Report **37**, 148 p, (1974).

78. Tatar, M., Hatzfeld, D. and Ghafori-Ashtiany, M. Tectonics of the Central Zagros (Iran) deduced from microearthquake seismicity. Geophys. J. Int**., 156**, 255–266 (2004).

79. Tatar, M., Hatzfeld, D., Martinod, J., Walpersdorf, A., Ghafori-Ashtiany, M. and Ch´ery, J. The present-day deformation of the central Zagros from GPS measurements. Geophys. Res. Lett., **9(19),** 1927, doi: 10.1029/2002GL015427 (2002).

80. Tecplot, Inc. Tecplot User's Manual Version 10. Bellevue, Washington (2005).

81. Tchalenko, J. S. Similarities between shear zones of different magnitudes. Geol. Soc. Am. Bull., v**. 81**, p. 1625-1640 (1970).

82. Teyssier, C., Tikoff, B., and Markley, M. Oblique plate motion and continental tectonics. Geology: v. **23 (5),** p. 447–450 (1995).

83. Tikoff, B. and Teyssier, C. Strain modelling of displacement-field partitioning in transpressional orogens, J. Struct. Geol., **16,** 1575–1588 (1994).

84. Vernant, P., and Ch´ery, C. Mechanical modelling of oblique convergence in the Zagros. Iran. Geophys. J. Int. **165**, 991–1002 (2006).

85. Vernant, P., et al. Present-day crustal deformation and plate kinematics in the Middle East constrained by GPS measurements in Iran and northern Oman, Geophys. J. Int., **157**, 381 – 398 (2004).

86. Vilotte, J.P., Daignieres, M., and Madariaga, R. Numerical modeling of intraplate deformation: simple mechanical models of continental collision. Journal of Geophysical Research **87 (B13),** 10709-10728, (1982).

87. Vilotte, J.P., Madariaga, R., Daignieres, M., and Zienkiewicz, O.C. Numerical study of continental collision: influence of buoyancy forces and an initial stiff inclusion. Geophysical Journal of the Royal Astronomical Society **84,** 279-310, (1985).

88. Walker, R., and Jackson, J. Active tectonics and late Cenozoic strain distribution in central and eastern Iran. TECTONICS, vol. **23**, TC5010, doi: 10.1029/ 2003TC001529, (2004).

89. Walpersdorf, A., Hatzfeld, D., Nankali, H., Tavakoli, F., Nilforoushan, F., Tatar, M., Vernant, P., Ch'ery, J., and Masson, F. Differences in the GPS deformation pattern of North and Central Zagros (Iran). Geophys. J. Int. **167,** 1077-1088 (2006).

90. Wang, K. Coupling of Tectonic Loading and Earthquake Fault Slips at Subduction Zones. PAGEOPH, Vol. **145,** Nos. 3/4, 537-559 (1995).

91. Wibberley, C.A.J., Yielding, G., and Di Toro, G. Recent advances in the understanding of fault zone internal structure: a review, Geological Society, London, Special Publications; v. **299**; p. 5-33 (2008).

92. Wiens, D.A., and Snider, N.O. Repeating deep earthquakes: evidence for fault reactivation at great depth. Science **293** (5534), 1463– 1466 (2001).

93. Woodcock, N.H. The role of strike-slip fault systems at plate boundaries. Philosophical Transactions of the Royal Society of London, **A317**, 13–27 (1986).